Journal of Scientific & Industrial Research
Vol. 83, December 2024, pp. 1373-1388
DOI: 10.56042/jsir.v83i12.8945

Spectroscopic Investigations, Quantum Chemical, Molecular Docking and Drug Likeness Studies of 3-Fluorobenzamide

S Sumathi, S Jeyavijayan* & N Karthik

Department of Physics, Kalasalingam Academy of Research and Education, Krishnankoil 626 126, Tamil Nadu, India

Received 20 February 2024; revised 25 July 2024; accepted 23 September 2024

A significant class of pharmaceuticals due to their biological properties and anti-tumor properties are benzamide derivatives. Density Functional Theory (DFT) calculations involving basis sets, 6-31++G(d,p) and 6-311++G(d,p), have been employed to understand the molecular characteristics of 3-fluorobenzamide. The FTIR and FT-Raman spectroscopies have been used to characterize the vibrational spectra of the molecule. The estimated structural parameters and vibrational frequencies have been analyzed and compared with the experimental findings. The frontier orbital energy gap of the molecule is determined to be 5.521 eV. According to UV-Vis study, the $\pi \rightarrow \pi^*$ transition occurs because the ring's C-C bonds function as a leading electron acceptor, while the oxygen (O13) and nitrogen (N14) atoms can act as electron donors. The density of states (DOS) spectrum has 84 electrons, 42α and 42β electrons combined. The Natural Bond Orbital (NBO) results showed that the lone pair transition of F8 and N14 atoms to π^*(C3-C4) and π^*(C12-O13) indicated a significant stabilizing energy of 17.84 and 43.56 Kcal·mol^{-1}. The region around the oxygen atom (electrophilic) and amino group hydrogen atoms (nucleophilic) have been analyzed. For ^{1}H and ^{13}C NMR, the predicted chemical shifts were 1.55 to 8.95 ppm and 127.04 to 193.09 ppm, respectively. The binding energies of human matrix metalloproteinase-2, an inhibitor of ovarian cancer, were found to be −6.5 Kcal·mol^{-1}, those of human progesterone and allosteric inhibitor, inhibitors of breast cancer, to be −6.6 and −5.4 Kcal·mol^{-1}, and those of histone deacetylases, an inhibitor of leukemia cancer, to be −6.5 Kcal·mol^{-1}, These are comparable to the binding energies of standard drugs (cytarabine, anastrozole, and carboplatin). ADMET predictions have been employed and the chemical can effectively cure cancers of the ovaries, breast and leukemia while reducing the adverse effects of medical procedures.

Keywords: Cancer treatment, Density functional theory, Docking, Drug likeness, 3-Fluorobenzamide

Introduction

Benzamide is an aromatic amide made up of one carboxamido substituent on benzene. Proteins are characterized by amide connections, which are partly responsible for the secondary structure of proteins due to amides' capacity to form hydrogen bonds. In a biological setting, amide connections that occur in a protein's main chain are referred to as peptide bonds, and those that occur in a protein's side chain as isopeptide bonds.[1] A number of medications, such as lysergic acid diethylamide, penicillin, and paracetamol, are amides. N-alkylamides found in plants also have a variety of biological uses.[2] It has been suggested that certain acetamide derivatives may have antibacterial action.[3] Particularly, the use of halogenated benzamide derivatives as radiotracers has proven to be beneficial in the diagnosis of dopaminergic neurotransmission disorders.[4] Researchers have examined the DFT investigations of benzamide derivatives, according to recent literature.[5,6] Furthermore, a number of studies have looked at the anti-cancer properties of benzamide derivatives.[7,8] The pharmaceutical industries have seen a significant increase in the use of DFT computations to understand vibrational and structural properties of the molecules. Therefore, for the first time, results from structural and quantum chemical computations of 3-fluorobenzamide (3FBA) have been provided by DFT calculations in conjunction with vibrational spectroscopy studies.[9] Also, there haven't been any reported molecular docking studies or quantum chemistry calculations of 3FBA in the literature. Hence, the optimized geometrical parameters, Molecular Electrostatic Potential (MEP), Mulliken charges, Fukui functions and Lowest Unoccupied Molecular Orbital (LUMO) and Highest Occupied Molecular Orbital (HOMO) energy gap have been carried out using DFT/B3LYP with 6-31++G(d,p) and 6–311++G(d,p) basis sets. The DOS spectrum has been used to characterize each border molecular orbital, and the 3FBA's electronegativity, hardness, chemical softness, and electrophilicity index have all been

*Author for Correspondence
E-mail: sjeyavijayan@gmail.com

established. It has been shown that the intra and the intermolecular interactions of the chemical are revealed by the NBO of the molecule. Furthermore, the Mulliken charges and Fukui functional values have been calculated for 3FBA. The gauge-independent atom orbital approach has been used to determine the NMR shift for ^{1}H and ^{13}C for 3FBA. Docking analysis has been used to establish the pharmacological properties of the therapeutic molecule 3FBA as well as its binding affinity with inhibitors of ovarian, breast and leukemia cancer. These results are similar to the binding affinities of conventional medications and 3FBA's biological potentials are being evaluated using ADMET testing.

Experimental and Computations

Experimental Characterizations

The sample 3FBA, which has a stated purity of 98%, was obtained from the Sigma-Aldrich Company. The chemical was measured at room temperature using a BRUKER IFS-66V vacuum Fourier transform spectrometer equipped with a mercury cadmium telluride (MCT) detector, a KBr beam splitter, and a globar source, providing a resolution of 1 cm^{-1}. With a FRA-106 FT-Raman attachment, the same interferometer was used to record the FT-Raman spectrum of 3FBA. The spectra in the 4000-50 cm^{-1} Stokes region have been obtained using the 200 mW power Nd: YAG laser in the 1064 nm line.

Quantum Computational Details

In order to satisfy the demands of precision and computational efficiency, theoretical approaches and foundational sets must be taken into account. When it comes to handling the electrical structure of molecules, DFT has proven to be quite helpful. With no restrictions on the geometry, the Gaussian 09 suite program package was used to calculate the molecular structure optimization of 3FBA and the corresponding vibrational harmonic frequencies using the DFT method with Becke-3-Lee–Yang–Parr (B3LYP) combined using a standard 6-31++G(d,p) and 6-311++G(d,p) basis sets.[10] The structural parameters of the title molecule have been tuned prior to the computation of vibrational wave numbers, chemical shifts, and electronic properties. Combining the results with these GAUSSVIEW[11] and VEDA[12] programs yielded the vibrational wave numbers. Through the vibrational frequency calculations of 3FBA, differences in thermodynamics parameters (entropy, heat capacity, and vibrational energy) have been evaluated. The time-dependent DFT approach has been used to determine electronic transitions, oscillator strengths, absorbance, and energy of vertical excitation. The B3LYP/6-311++G(d,p) method has been used to assess the MEP, HOMO, and LUMO energy of the chemical in question as well as its reaction sites. Through NBO calculations, intermolecular delocalization has been carried out to understand different second order interactions between full orbitals and empty orbitals.[13] One of the most often used techniques for calculating atomic magnetic shielding tensors is the GIAO method,[14] which yields the ^{13}C and ^{1}H NMR chemically shifts. The GaussSum[15] has also been used to prepare the Total Density of States (TDOS) spectrum, aside from these calculations. The charge contributions to each atom in the molecule have been assessed using Mulliken population analysis.

Molecular Docking and ADMET

The activation of multiple cells downstream signaling pathways by an estrogen and progesterone receptors leads to the development and spread of cancer. Using a computer-based molecular simulation method, we assessed the inhibitory potential of 3FBA against cancers marker proteins. In the docking study of 3FBA, the ovarian, breast and leukemia cancer receptors have been investigated. Protein markers for cancer have been identified using human matrix metalloproteinase-2 (MMP-2) (PDB ID: 7XJO and PDB ID: 7XGJ) receptors for ovarian cancer, human progesterone (PDB ID: 4OAR) and allosteric inhibitors (PDB ID: 5KCV) receptors for breast cancer and histone deacetylases (PDB ID: 5EDU) for leukemia cancer. The PyMOL, which molecule graphics system[16] has been used to demonstrate the position of protein and ligand (3FBA) interaction. Auto Dock Vina[17] (Version: 4.2.1) has been utilized for molecular docking analysis. Before molecular docking, Discovery Studio[18] (Version: 2017 R2 client) was used to analyze the protein structure and amino acid positions. We used one of the public ligand databases, PubChem (http://pubchem.ncbi.nlm.nih.gov), to extract the structure of the ligand 3FBA.[19] In order to ascertain the pharmacodynamic activities in our human body, a pharmacological sketch known as "adsorption, distribution, metabolism, and toxicity" (ADMET) is utilized. There are currently a number of offline and online software tools available to assist in predicting drug use. In this research, the biological activities

were strengthened by the use of the ADMET-SAR[20] and SwissADME[21] tools.

Results and Discussion

Molecular Geometry Analysis

The composition of 3-fluorobenzamide is shown in Fig. 1. Using the 6-31++G(d,p) and 6-311++G(d,p) basis sets, DFT/B3LYP method is used to calculate the optimal structural parameters (bond length and bond angle), which are shown in Table 1. Data from experiments are compared with these findings.[22] One C = O bond, seven C–C bonds, four C–H bonds, one C–F bond, one C–N link, two N–H bonds are found in the title molecule. A comparison of bond lengths and bond angles across the basis sets for 3FBA demonstrates that the B3LYP/6-31+G(d,p) level of theory generally overestimates bond lengths, it produces bond angles that are very close to those obtained by B3LYP with 6-311++G(d,p) technique. For the lower and higher basis sets, the 3FBA least optimized energy is expected to be −500.225222 and −500.338310 Hartrees, respectively. The C2-H7, C4-H9, C5-H10 and C6-H11 bond lengths of 3FBA have been calculated by larger basis set as 1.083, 1.083, 1.082 and 1.009 Å, these are well matched with the experimental XRD data (0.95 Å). The 3FBA's C-C bond lengths are calculated between 1.356 and 1.505 Å, the corresponding experimental bond lengths lying between 1.386 and 1.515 Å. This clearly indicates that there hasn't been any delocalization of the π-electrons surrounding these bonds. The bond lengths of N14-H15, N14-H16 and C3-F8 in 3FBA are determined to be 1.007, 1.084 and 1.395 Å, respectively. These values are in good agreement with the experimental values of 0.880, 0.880 and 1.361 Å. With experimental values of 1.359 and 1.252 Å, the bond lengths of C12-N14 and C12-O13 are found to be 1.371 and 1.219 Å, respectively. The Oxygen (O13) atom joined at C12 result in bond angles of C2-C1-C12 (122.6°) is being larger than normal C-C-C angles. This variation in bond angle is determined by the electronegativity of atom O13, since the bond angle increase with increasing electronegativity. DFT computations yielded the following bond angles:

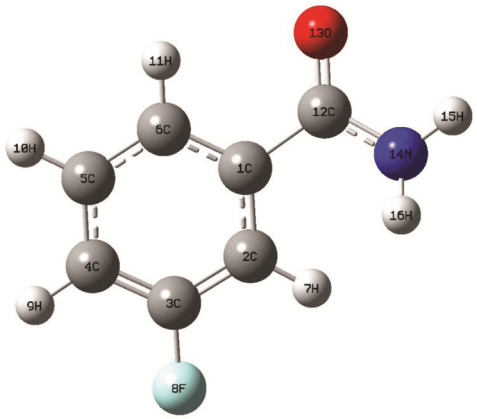

Fig. 1 — Optimized structure of 3-fluorobenzamide

Table 1 — The optimized structural parameters of 3-fluorobenzamide

Bond length (Å)	Structural parameters		
	6-31++G(d,p)	6-311++G(d,p)	Experimental [22]
C1-C2	1.403	1.398	1.406
C1-C6	1.402	1.385	1.404
C1-C12	1.505	1.505	1.515
C2-C3	1.388	1.386	1.386
C2-H7	1.085	1.083	0.950
C3-C4	1.389	1.356	1.393
C3-F8	1.360	1.395	1.361
C4-C5	1.398	1.391	1.403
C4-H9	1.085	1.083	0.950
C5-C6	1.395	1.398	1.394
C5-H10	1.086	1.082	0.950
C6-H11	1.084	1.009	0.950
C12-O13	1.227	1.219	1.252
C12-N14	1.372	1.371	1.359
N14-H15	1.010	1.007	0.880
N14-H16	1.008	1.084	0.880
Bond angle (°)			
C2-C1-C6	119.7	119.7	120.7
C2-C1-C12	122.6	122.6	122.4
C6-C1-C12	117.7	117.7	116.9
C1-C2-C3	118.6	118.7	117.8
C1-C2-H7	122.5	122.4	121.1
C3-C2-H7	118.9	118.9	118.5
C2-C3-C4	122.8	122.6	123.0
C2-C3-F8	118.4	118.5	118.6
C4-C3-F8	118.8	118.9	118.4
C3-C4-C5	118.1	118.2	118.3
C3-C4-H9	119.9	119.8	120.9
C5-C4-H9	122.1	122.0	120.9
C4-C5-C6	120.6	120.6	120.4
C4-C5-H10	119.5	119.5	119.8
C6-C5-H10	119.9	120.0	119.8
C1-C6-C5	120.2	120.2	120.1
C1-C6-H11	118.5	118.6	119.8
C5-C6-H11	121.2	121.2	120.1
C1-C12-O13	121.7	121.7	120.2
C1-C12-N14	116.6	116.3	116.1
O13-C12-N14	121.7	122.0	123.9
C12-N14-H15	116.2	116.3	119.4
C12-N14-H16	121.6	121.3	121.2
H15-N14-H16	117.4	117.4	118.4

122.6°, 118.5°, 121.2°, 116.3°, 117.4° and 121.0° for C2-C3-C4, C2-C3-F8, C5-C6-H11, C1-C12-N14, H15-N14-H16, and O13-C12-N14 (corresponding to experimental values are 123.0°, 118.6°, 120.1°, 116.1°, 118.4° and 123.89°). Both the bond lengths and bond angles, which have been computed using various basis sets, match well with the results of experiment.

Thermodynamic Parameters

We have used B3LYP method to determine the fundamental statistics thermodynamics functions, heat capacity and entropy, for 3FBA, from the theoretical harmonic frequencies. These are presented in Table 2. We have calculated the rotational constants, entropy, zero-point vibrational energies (ZPVE), and the variations in the ZPVEs seem to be small. According to lower and higher basis sets, the ZPVE for 3FBA is 74.525 and 74.766 Kcal·mol^{-1}, respectively. If the molecules have high dipole moment values, there will be more intermolecular interactions. Here, the total dipole moment of 3FBA has been found to be 2.367 and 2.331 Debye by both basis sets. For B3LYP, the rotational constants increases in value as one move from lower to higher basis sets. In the thermochemical discipline, these parameters can be applied to estimate chemical reaction directions based on the second law of thermodynamics and compute other thermodynamic energies based on correlations between thermodynamic functions.

Table 2 — The thermodynamic parameters of 3-fluorobenzamide

Parameters	DFT-B3LYP/ 6-31++G(d,p)	DFT-B3LYP/ 6-311++G(d,p)
Optimized global minimum Energy (Hartrees)	−500.225222	−500.338310
Total energy (thermal), E_{total} (Kcal·mol^{-1})	80.036	79.793
Heat capacity, C_v (cal mol^{-1} k^{-1})	32.255	32.252
Total Entropy, S (cal mol^{-1} k^{-1})	90.537	90.510
Translational Entropy (cal mol^{-1} k^{-1})	2.981	2.981
Rotational Entropy (cal mol^{-1} k^{-1})	2.981	2.981
Vibrational Entropy (cal mol^{-1} k^{-1})	20.180	20.165
Vibrational energy, E_{vib} (Kcal·mol^{-1})	78.258	78.016
Zero-point vibrational energy, (Kcal·mol^{-1})	74.766	74.525
Rotational constants (GHz)		
A	2.606	2.616
B	0.919	0.922
C	0.688	0.692
Dipole moment (Debye)	2.367	2.331

Vibrational Analysis

All 42 normal modes of 3FBA have been calculated by both lower and higher basis sets and are listed in Table 3. The FTIR and FT-Raman spectra of 3FBA are shown in Figs. 2 and 3. A solid-state molecule is the subject of the experimental data, whereas an isolated gaseous phase molecule is the subject of the theoretical calculations. As a result, it is observed that the vibrational frequencies differ slightly from the experimental data. Hence, the estimated wave numbers are scaled with the scale factor[23] of 0.9613 for the B3LYP technique.

Amide Group Vibration

The 3450-3250 cm^{-1} region is distinctive for the quick identification of the vibrations associated with N-H stretching.[24] The type of the substituent has no discernible effect on the bands in this region. The asymmetric and symmetric NH_2 stretching modes of 3FBA have been identified at 3405 and 3365 cm^{-1} in Raman and IR spectra, respectively. The corresponding scaled values are found as 3567 and 3447 cm^{-1} by large basis set. These vibrations have 100% and 98% PED values, indicating that they are pure modes. For scissoring deformation, the amide group frequencies appear between 1650 and 1615 cm^{-1}, while for rocking deformation, they appear between[24] 1100 and 1000 cm^{-1}. The Raman band at 1675 cm^{-1} and FTIR at 1668 cm^{-1} are assigned as NH_2 scissoring mode of 3FBZ and its rocking vibration is measured at 1010 cm^{-1} in FTIR. Based on 76% of PED data, the wagging mode of amino group for 3FBA has been determined to be at 499 cm^{-1} in IR and 480 cm^{-1}in FT-Raman. The scaled B3LYP/6-311++G(d,p) technique and the vibrations displayed in Table 3 correspond quite well.

C-H Vibrations

The heteroaromatic structure exhibits C-H stretching vibration in the region[25] of 3100–3000 cm^{-1}. In the current investigation, the C-H vibrations of the title compound have been assigned to C-H stretching vibrations at 3190, 3086 cm^{-1} in IR and at 3120, 3100, 3030 cm^{-1} in the Raman spectrum (93–97% PED). In aromatic compounds, the C-H in-plane and out-of-plane bending vibrations are lie in the range of 1000–1300 cm^{-1} and 950–800 cm^{-1}, respectively.[25] The C-H in-plane bending vibrations in 3FBZ are detected at 1147, 1084, and 950 in IR. The

corresponding Raman vibrations are detected at 1150 and 1000 cm^{-1}. The scaled DFT frequencies are in good agreement with these results. The C–H out-of-plane vibrations 3FBA have also been identified and are listed in Table 3.

Ring Vibrations

Due to the conjugate substituent's presence, the carbon atom in the benzene ring experiences coupled vibration, resulting in the maximal C-C stretching modes that are visible in the 1660–1420 cm^{-1} range.[25]

Table 3 — The calculated vibrational frequencies (cm^{-1}), IR intensities (Km mol^{-1}), Raman scattering activity ($Å^4$ amu^{-1}), reduced mass (amu), force constants (mDyne/$Å^{-1}$) and vibrational assignments based on PED calculations for 3-fluorobenzamide

S. No	Observed wave number(cm^{-1})		Calculated Wavenumber (cm^{-1})								Assignment with PED (%)
			DFT-B3LYP/6-31++G(d,p)				DFT-B3LYP/6-311++G(d,p)				
	FT-IR	FT- Raman	Unscaled	Scaled	IR Intensity	Raman activity	Unscaled	Scaled	IR Intensity	Raman activity	
1	—	3405(vw)	3728	3584	41	55	3711	3567	40	50	NH_2 ass (100)
2	3365(s)	—	3595	3456	45	158	3586	3447	45	158	NH_2ss (98)
3	3190(ms)	3120(ms)	3228	3103	3	128	3209	3085	3	136	νCH(97)
4	—	3100(s)	3221	3097	1	121	3202	3079	1	109	νCH(95)
5	3086(vw)	—	3216	3092	1	66	3197	3074	1	65	νCH(96)
6	—	3030(vw)	3199	3075	7	79	3181	3058	6	71	νCH(93)
7	1668(vw)	1675(vw)	1754	1686	319	44	1748	1681	332	42	NH_2sciss(70)
8	1594(s)	1600(vs)	1657	1593	1	68	1648	1585	1	64	νC=O(87)
9	—	1575(w)	1634	1570	105	2	1626	1563	107	2	νCC(85)
10	—	—	1624	1561	144	11	1621	1558	132	11	νCC(86)
11	1480(vw)	1490(vw)	1522	1463	27	1	1516	1457	28	1	νCC(84)
12	—	1425(w)	1468	1411	25	1	1462	1405	26	1	νCC(82)
13	1378(ms)	—	1371	1318	191	31	1360	1307	239	34	νCC(81)
14	—	1290(vw)	1360	1308	73	9	1346	1294	25	3	νCC(80)
15	1273(ms)	1250(vs)	1306	1255	16	42291	1300	1250	19	5	νCN(80)
16	1189(vw)	1175(vw)	1241	1193	107	13	1234	1186	112	13	νCC(81)
17	1147(ms)	1150(ms)	1182	1136	3	4	1180	1134	3	4	bCH (79)
18	1084(vw)	—	1126	1083	3	3	1122	1079	3	3	bCH (78)
19	1010(vw)	—	1104	1061	3	11	1103	1060	2	11	NH_2 rock(85)
20	—	1000(vs)	1080	1038	11	4	1078	1036	15	3	bCH (77)
21	950(ms)	—	1017	978	0	39	1017	978	0	38	bCH (76)
22	930(w)	—	998	959	1	0	997	959	1	0	R trigd(75)
23	918(ms)	—	932	896	0	0	931	895	0	0	R symd(74)
24	—	—	923	887	31	2	920	884	33	2	bCN(75)
25	830(ms)	—	890	856	19	0	894	859	19	1	R asymd(75)
26	—	768(vw)	816	784	20	0	818	786	15	0	bCC(74)
27	—	720(vw)	764	734	52	1	768	738	56	1	νCF(72)
28	670(ms)	700(vw)	726	698	12	14	726	698	13	14	ωCH(64)
29	664(ms)	672(vw)	682	656	5	0	688	662	8	0	ωCH(63)
30	598(s)	624(vw)	628	604	22	1	631	607	22	1	ωCH(63)
31	576(vw)	—	581	559	19	1	581	559	18	1	ωCH(62)
32	532(ms)	528(ms)	544	523	6	1	546	525	7	1	bCF(61)
33	499(w)	480(vw)	518	498	5	4	519	499	6	4	NH_2 wag(76)
34	444(vw)	—	484	465	5	1	484	466	5	1	bC=O(71)
35	—	396(vw)	427	411	17	0	427	411	15	0	ωCC(60)
36	—	372(vw)	394	379	16	1	394	379	12	1	ωCF(57)
37	—	—	366	352	132	3	366	352	137	3	ωCN(60)
38	—	348(vw)	359	345	33	2	359	345	27	2	tRtrigd(62)
39	—	240(s)	244	235	0	2	244	234	0	2	ωC=O(63)
40	—	174(vw)	186	179	8	0	186	179	8	0	tRsymd(64)
41	—	150(vw)	146	140	3	2	146	140	3	2	tRsymd(64)
42	—	—	56	54	11	1	56	54	10	1	NH_2 twist(60)

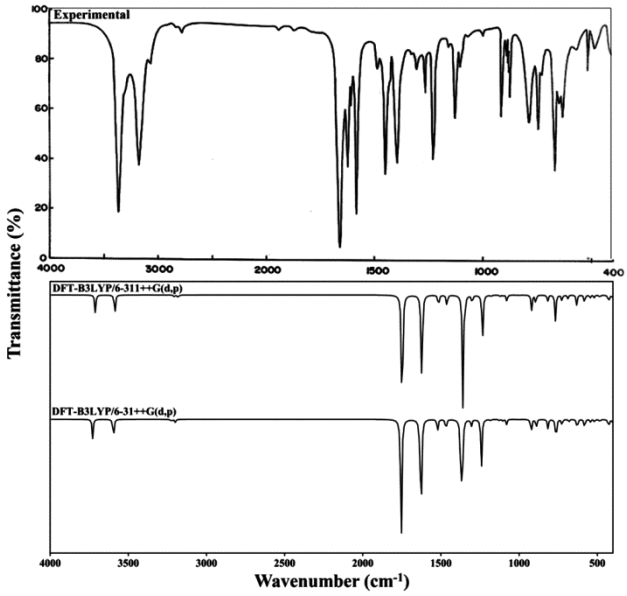

Fig. 2 — Comparison of observed and calculated IR spectra of 3-fluorobenzamide

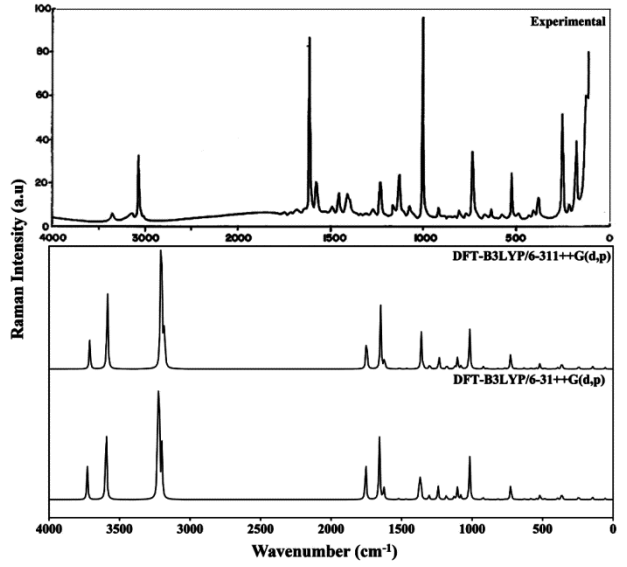

Fig. 3 — Comparison of observed and calculated FT-Raman spectra of 3-fluorobenzamide

In 3FBA, the C-C stretching modes are attributed to the bands at 1480, 1378, 1189 in the FTIR and 1575, 1490, 1425, 1290, 1175 cm^{-1} in FT-Raman spectrum (80–86% PED). The C-C bending vibrations, both in-plane and out-of-plane, are typically measured between 1000–675 cm^{-1} and 450–112 cm^{-1}, respectively. Both in-plane and out-of-plane bending vibrations of 3FBZ are observed between 930–830 cm^{-1} and 348–150 cm^{-1} and are reported in Table 3 with their PED values.

C-N, C=O and C-F Vibrations

It is exceedingly challenging to identify C-N vibrations because of the blending of several bands. The range 1382–1266 cm^{-1} has been classified as the C-N stretching absorption.[26] The C-N stretching vibration of 3FBZ has been attributed to the mode seen at 1273 cm^{-1} in FTIR and 1250 cm^{-1} in FT-Raman spectrum (80% PED). Within the range of 1850–1600 cm^{-1}, the C=O stretching vibrations can be seen. The FT-Raman spectrum's band acquired at 1600 cm^{-1} and the IR band found at 1594 cm^{-1} are assigned for C = O stretching vibration of 3FBZ with 87% PED. The scaled B3LYP frequencies by large basis set agree well with the observed results. It is challenging to identify the C–F stretching modes which are caused by interaction with other bending modes of vibration. Many fluorobenzenes in the range of 1000–1300 cm^{-1} include C–F stretching modes that are closely related to C–H in-plane bending vibrations.[25] In 3FBA, the Raman spectrum shows a C-F stretching vibration at 720 cm^{-1} (72% PED). Usually, the range of 250 to 350 cm^{-1} is used to measure the C–F in the plane bending vibration. The vibrational spectra of 3FBA show that the C-F in the plane has been found at 532 and 528 cm^{-1}, respectively, while the Raman spectrum shows that the out-of-plane vibrations is at 372 cm^{-1}.

Frontier Molecular Orbitals (FMO)

The optical and electrical characteristics of organic compounds are frequently explained through the use of FMO analysis.[24] Understanding the energy of the HOMO and LUMO and their associated characteristics is crucial for determining a molecule's chemical reactivity. When molecules interact, the LUMO is an electron acceptor whose energy is correlated with the electron affinity (EA) while the HOMO is an electron donor whose energy is correlated with the ionization potential (IP).[25,26] In this study, the oxygen (O13) and nitrogen (N14) atoms in the ring can function as the electron donor whereas the C-C bonds of ring act as a leading electron acceptor for 3FBZ. The HOMO and LUMO energies are calculated as −7.27 eV and −1.75 eV, respectively, and the energy gap is found to be 5.5219 eV in the gas phase, by B3LYP/6-311++G(d,p) computation. The boundary orbitals for 3FBA are displayed in Fig. 4. The solvents were found to have a considerable effect on the energy gaps. The methanol and ethanol phases have HOMO-LUMO energy values of −7.29 and −1.73 eV, respectively, which

deviate from the gas phase calculations, leading to larger energy gaps. As a result, the energy gap widens and the molecule becomes more stable as it transitions from the gas to the solvent phase. The energy gap across HOMO and LUMO in the gas phase of 3FBA is 5.52 eV, and it is less than that of methanol and ethanol (polar: 5.57 eV) by large basis set calculations. In conclusion, reduced chemical reactivity and better kinetic stability are reflected in a wide energy gap. Using Koopman's relations[27] in the DFT calculations, the global reactivity properties of 3FBA and conventional medications are displayed in Table 4. It is discovered that the reactivity parameters are comparable to those of standard medications. The

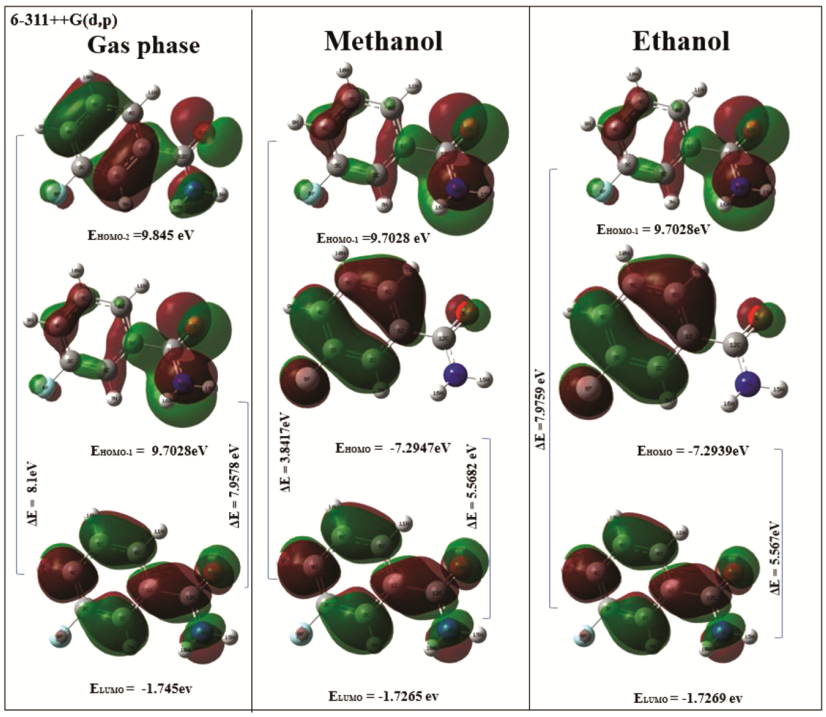

Fig. 4 — HOMO-LUMO plot of 3-fluorobenzamide

Table 4 — Global reactivity descriptors for 3-fluorobenzamide and standard drugs

Molecular Properties	3-fluorobenzamide			Carboplatin			Anastrozole			Cytarabine		
	Gas phase	Methanol	Ethanol	Gas phase	Methanol	Ethanol	Gas phase	Methanol	Ethanol	Gas phase	Methanol	Ethanol
HOMO (eV)	−7.27	−7.29	−7.29	−7.82	−8.00	−7.99	−7.54	−7.34	−7.34	−6.48	−6.79	−6.73
LUMO (eV)	−1.75	−1.73	−1.73	−1.03	−1.14	−1.14	−1.61	−1.3	−1.31	−1.03	−1.21	−1.14
ΔE (E_{HOMO} -E_{LUMO}) (eV)	5.52	5.57	5.57	6.79	6.85	6.85	5.93	6.04	6.04	5.45	5.57	5.59
Ionization potential (I) (eV)	7.27	7.29	7.29	7.82	8.00	7.99	7.54	7.34	7.34	6.48	6.79	6.73
Electron affinity (A) (eV)	1.75	1.73	1.73	1.03	1.14	1.14	1.61	1.3	1.31	1.03	1.21	1.14
Globalhardness (η) (eV)	2.76	2.78	2.78	3.40	3.43	3.43	2.97	3.02	3.02	2.72	2.79	2.79
Global softness (s) (eV^{-1})	0.18	0.18	0.18	0.15	0.15	0.15	0.17	0.17	0.17	0.18	0.18	0.18
Electronegativity (χ) (eV)	4.51	4.51	4.51	4.42	4.57	4.57	4.57	4.32	4.33	3.75	4.00	3.94
Chemical potential (μ) (eV)	−4.51	−4.51	−4.51	−4.42	−4.57	−4.57	−4.57	−4.32	−4.33	−3.75	−4.00	−3.94
Global electrophilicity (w) (eV)	3.68	3.65	3.65	2.88	3.05	3.04	3.53	3.09	3.1	2.58	2.87	2.77

molecular system's hardness (η), electronegativity (χ), and chemical potential (μ) validate the high chemical reactivity of 3FBA. In contrast to hard molecules, which have large energy gaps, soft molecules have low energy gaps. By employing large basis set computations, it is found that 3FBA has a chemical hardness of 2.76 eV and a chemical softness of 0.18 eV^{-1} in the gas phase. In methanol and ethanol, the 3FBA chemical hardness and softness values are 2.78 eV/0.18 eV^{-1} and 2.78 eV/0.18 eV^{-1}, respectively. Organic compounds can be classified as moderate electrophiles ($0.8 < \omega < 1.5$ eV), strong electrophiles ($\omega > 1.5$ eV), or marginal electrophiles ($\omega < 0.8$ eV) using the established electrophilicity (ω) scale.[27] The electrophilicity index (ω) of 3FBA in the solvents and gas phase were found to be 3.65 eV and 3.68 eV, respectively. These results indicated the chemical's potential as an effective electrophile. The UV/Vis spectrum of 3FBA has been computed in methanol and ethanol to investigate the effects of the solvent on its electronic structure and molecular geometries. For gas and solvent phases, the oscillator power, the wavelength, excitation energies, and major contributions have been determined and are displayed in Table S1 (Supplementary). With excitation energies of 4.492, 4.911, and 5.517 eV, respectively, the electronic absorption band of 3FBA in gas phase has been found at 276.0 nm (H−1→L contributes 46.66%), 252.5 nm (H−1→L contributes 41.38%), and 224.7 nm (H−2→L contributes 66.66%). The 3FBA sample in methanol had distinct bands at e = 4.703, 4.906, and 5.440 eV, respectively, at 263.6 nm (H→L contributes 38.05%), 252.7 nm (H→L contributes 42.69%), and 227.9 nm (H−1→L contributes 40.86%). In ethanol, three absorption bands have been determined using e = 4.699, 4.904, and 5.438 eV, respectively, at 263.9 nm (H−L contributes 38.01%), 252.8 nm (H→L contributes 42.91%), and 228.0 nm (H−1→L contributes 41.48%). The calculated absorption peaks are displayed in Fig. S1 (Supplementary).

DOS Spectrum

It might not always be useful to describe border orbitals just in terms of the 3FBZ's HOMO and LUMO. Similar degenerate energy levels could exist for neighboring orbitals in the border zone. To obtain the DOS, the electron densities of states, alpha (α) and beta (β), are combined together.[28] Gaussian curves and molecular orbital data are combined using the GaussSum 3.0 tool[15] to construct these. The density of state plot is used to show the composition of the gap in energy and boundary orbitals of the system. Molecular orbital configurations and how they affect molecule chemical bonding are depicted in Fig. S2 (Supplementary). A total of 84 electrons are involved in DOS since 3FBA is made up of 42 and 42β electrons. The LUMO and HOMO energy levels are shown as red and green bars, respectively. The computed HOMO energy is −7.27 eV, whereas the LUMO energy is −1.75 eV. The energy gap between the LUMO and HOMO, which is 5.52 eV, reflects the findings of UV-Vis study. The energy levels of the orbitals are altered due to substitutions and modifications in the bonding properties inside the ring's C-C bond, which shifts the DOS peaks. This is an indication of the molecule's electrical structure and chemical reactivity.

NBO Analysis

To comprehend different second order interactions between the full and vacant orbitals, and to execute intermolecular delocalizations, the NBO computations were carried out using the Gaussian 09 software. To assess the donor-acceptor interactions, the Fock matrix[29] in the NBO basis of 3FBA has been analyzed using second order perturbation theory. A loss of occupancy from the localized NBO of the idealized Lewis structure into an empty non-Lewis orbital is the outcome of the interactions. The stabilization energy E_2 connected to the delocalization i→j is approximated for every donor (i) and acceptor (j) as

$$E_2 = \Delta E_{ij} = q_i \frac{F(i,j)^2}{\varepsilon_i - \varepsilon_j}$$

The donor orbital occupancy is denoted by q_i, the diagonal elements are ε_i and ε_j, and the Fock matrix NBO element is represented by F(i,j). NBO investigation for 3FBA at the DFT/B3LYP/6-311++G (d,p) level has been done and are listed in Table S2 (Supplementary). The orbitals in 3FBA that have the highest stabilization energies are π(C1-C2)→π*(C3-C4), π(C1-C2)→π*(C5-C6), π(C1-C2)→π*(C12-O13), π(C3-C4)→π*(C1-C2), π(C3-C4)→π*(C5-C6) and π(C5-C6)→π*(C1-C2), (22.25, 18.21, 15.14, 19.50, 18.97 and 21.97 Kcal·mol^{-1}). High electron densities are the result of those interactions in the C-C and C-O anti-bonding acceptor orbitals (approximately 0.36e, 0.31e, 0.27e, 0.38e, 0.31e, and 0.38e). These are key characteristics that set 3FBA apart chemically.

Mullikan Charge Analysis

The determination of effective atomic charge is a crucial step in applying quantum mechanical computations to molecular systems[28]. The electron population of each atom as determined by the basis function is used to calculate Mulliken atomic charges. The Mulliken atomic charges of 3FBA are included in Table S3 (Supplementary) and Fig. S3 (Supplementary). These charges were estimated at the B3LYP approach utilizing the basis sets 6-31++G(d,p) and 6-311++G(d,p).We have studied the Mulliken atomic charge of ethanol and methanol as well as 3FBA in the gas phase. The atom C1 (acceptor) had the most positive charge using the 6-311++G(d,p) basis set and B3LYP; this decreased from 1.279e in the gas phase to 1.223e in methanol and 1.224e in ethanol. Furthermore, it is demonstrated that the carbon atom C12 can act as a donor atom since their negative charges increase as they move from the gas phase (−0.089e) to the methanol (−0.042e) and ethanol (−0.043e). The charges on each hydrogen atom are all positive. Amino group hydrogens (H15 and H16) in particular have the highest positive charges, while the oxygen atom (O13) has a negative charge of −0.319e, −0.405e and −0.404e in gas phase, methanol and ethanol, respectively. Therefore, in 3FBA, a significant amount of changes in charge distribution and are due to the raising of dielectric coefficient of the solvents.

Fukui Function

The Fukui function, which shows how the electron density can alter at a specific site of both contribute or absorb electron that are more susceptible to attack by nucleophiles or electrophiles, respectively, is crucial for understanding chemical reactivity. Fukui functions have been computed for 3FBA for assaults involving radicals, electrophiles, and nucleophiles. Mulliken population analysis has been used to recreate the Fukui function from each individual atomic charge. The Fukui function[30] is computed using the electrophilic, nucleophilic, and free radical groups of 3FBA are as follows,

$$f_k^+ = q_j(N+1) - q_j(N)$$

$$f_k^- = q_j(N) - q_j(N-1)$$

$$f_k^0 = \frac{1}{2}[q_j(N+1) - q_j(N-1)]$$

where, the chemical species that are neutral (N), cationic (N−1) and anionic (N+1), $q_j$stands for the charge at the j^{th} site. The difference between the nucleophilic and electrophilic functions is the definition of the dual descriptor proposed by Morell *et al.*[31] and is given by equation,

$$\Delta f(r) = f_k^+ - f_k^-$$

The aforementioned three equations, which assess reactivity at atomic resolution, have been used to characterize the Fukui function and ascertain the pin point distribution of the atomic sites on 3FBA. In this study, the Fukui function of 3FBA at two basis sets, B3LYP/6-31++G(d,p) and B3LYP/6-311++G(d,p), has been determined via Mulliken charges. The dual descriptor distinguishes between nucleophilic and electrophilic attacks at a given site based on their sign. Considering the data presented in Table S4 (Supplementary), the dual descriptor's requirements are met by the electrophilic sites for 3FBA, which are C1, C3, C5, F8, C12, O13, and N14. On the other hand, the nucleophilicsites C2, C4, C6, H7, H9, H10, H11, H15 and H16 have negative values in both basis sets. These results are correlated with the maximum positive charges found in atoms H15 and H16 and the negative charges found in O13 according to the Mulliken charge analysis. During the process, depending on its local behavior, the molecule 3FBA responds to both nucleophilic and electrophilic assaults.

MEP Analysis

The responsive regions of the molecular bonding process can be illuminated with the use of MEP's different color codes.[32,33] The MEP surfaces for 3FBA have been estimated at B3LYP with both larger and smaller basis sets as shown in Fig. S4 (Supplementary). By establishing linkages with the chemically active areas of molecule, the MEP expands our understanding of substituent effects, electrophilic reactions, molecular reactivity, and inter-intra-molecular interactions. Green, blue, yellow, and red all have electrostatic potentials that get stronger with each color. In 3FBA, the electron-deficient (blue) part is encircled by hydrogen atoms (H15 and H16) of amino group, while the electron-rich (red) sections are produced by the lone pair of oxygen atom (O13). Consequently, there was a correlation between the Mulliken charge findings and Fukui function results of 3FBA. The C-C bonds in the ring structure (green) contain the neutrality electrostatic potentials of 3FBA. Furthermore, the intensity of the color changes from ethanol < gas phase; in other words, the red, blue and green patches on the oxygen, fluorine,

nitrogen, hydrogen and carbon atoms darken as one proceeds from ethanol to gas phase.

NMR Analysis

Using NMR simulation to determine the structure of massive macromolecules is one of the possible approaches in quantum chemistry. Using the DFT with GIAO approach, the ^{1}H and ^{13}C chemical shifts of 3FBZ in the gas phase, methanol, and ethanol have been computed.[34] The NMR shifts for 3FBA are shown in Table S5 (Supplementary) and Fig. S5 (Supplementary). For all carbon atoms, the computed shifts using the larger basis set are consistently higher than those obtained using computations with a smaller basis set. This is to be expected as higher basis sets often yield more accurate and occasionally greater chemical shift values due to an improved link between electrons and polarization functions. Usually, the presence of a liquid solvent (ethanol or methanol) causes deshielding, which causes more significant chemical changes than in the gas phase. For this effect, shifts increasing from conditions in the gas phase to those in the solvent are found in both basis sets. Here, the greatest predicted ^{13}C NMR shift in gas phase for C12 is 193.09 ppm since oxygen (O13) provides the least effective shielding. In methanol and ethanol solvents, the calculated shifts for C12 are 196.68 and 196.63 ppm, respectively. A little chemistry shifting in the gas phase is seen for the atom of carbon C2 at 127.04 ppm, which is likely caused by the neighboring fluorine nuclei (F8) having a stronger shielding effect. In 3FBZ, the chemical shifts of carbon C2 in methanol and ethanol solvents are 127.01 and 127.02 ppm, respectively. When directly connected hydrogen is positioned next to an electron-accepting atom, they create a greater wave number and have less shielding due to resonance. The resonance is driven to a lower wave number by approaching the electron donor to a greater extent because of improved shielding. The projected signal of H7 linked near the carbon atom (C2) thus reveals a maximum value of 8.95 ppm in the gas phase. In the case of the solvents methanol and ethanol, corresponding chemical shifts of 8.98 and 8.98 ppm have been found. Also, a minor shift of 1.55 ppm occurs in the gas phase when the hydrogen atom (H16) forms a bond by an electronegative atom (N14). In methanol and ethanol, the chemical shift of H16 is determined to be 1.90 ppm. The rise in the chemical shift might be due to hydrogen bonding or other solvation processes that don't exist in the gas phase.

Molecular Docking Study

In the area of pharmaceutical drug findings, chemical software known as molecular docking is used to analyze ligand and protein binding sites.[35,36] We have selected ovarian, breast and leukemia cancer proteins such as human matrix metalloproteinase-2 (MMP-2) (PDB ID: 7XJO and PDB ID: 7XGJ), human progesterone (PDB ID: 4OAR), allosteric (PDB ID: 5KCV) and histone deacetylases (PDB ID: 5EDU) inhibitors for the 3FBA docking calculations based on previous literatures.[37,38] The molecular docking investigations of 3FBZ are shown in Figs. 5(a), (b) and (c). All target proteins have been taken from the RCSB Protein Data Bank (http://www.rcsb.org/pdb). The X-ray crystallographic structures of anastrozole and carboplatin have been chosen by comparing them to the macromolecules of widely used drugs. Docking experiments have shown that hydrogen bonds and amino acid residues[39,40] inside target proteins can interact with the ligand molecule 3FBZ. Our findings indicate that 3FBA interacts with the 7XJO receptor via four common ALA A:140, ALA A:137, LEU A:138 and THR A:144 hydrogen bonds residues separated by 2.22 Å, 2.60 Å, 2.56 Å, and 2.97 Å, respectively, as shown in Table 5. Compared to typical medication (carboplatin), which has a binding affinity of −5.1 Kcal·mol^{-1}, the binding energy between 7XJO and 3FBA are found to be greater (−6.5 Kcal·mol^{-1}). Subsequent investigation showed that 3FBA and protein 7XGJ also establish a stronger hydrogen bond through three traditional hydrogen bonds, which are separated by 2.04, 2.82, and 2.31 Å, respectively, between ALA A:137, LEU A: 138, and THR A: 144. The binding affinity between the 7XGJ protein and 3FBA has been calculated as −6.5 Kcal·mol^{-1}. On the other hand, the hydrogen bond residues of 4OAR and 5KCV such as LEU A: 758 (2.92 Å), MET A: 759 (2.85 Å), LYS A:822 (2.40 Å) and GLN A: 414 (2.50 Å), ASP A:262 (2.48 Å), SER A:259 (2.82 Å) interacts with the ligand 3FBZ and exhibit substantial binding affinities of −6.6 and −5.4 Kcal·mol^{-1}, respectively, which are comparable with the binding affinity of standard drug, anastrozole (−5.9 Kcal·mol^{-1}). Similarly, the hydrogen bond residues of 5EDU, such as HIS A: 611(2.58 Å) and GLY A: 619(2.52 Å), have binding energies of −6.5 Kcal·mol^{-1} when they interact with the ligand 3FBA. This is comparable to the conventional medication cytarabine's binding affinity (−6.3 Kcal·mol^{-1}). As a result, the 3FBA ligand may able to inhibit the action

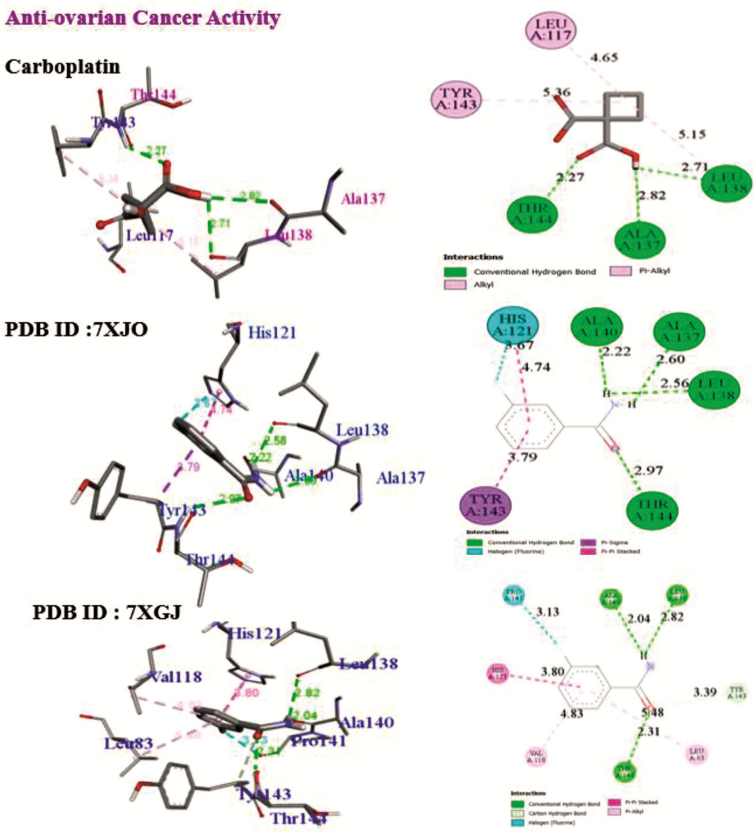

Fig. 5 — Interaction of 3-fluorobenzamide against: (a) anti-ovarian cancer, (b) anti-breast cancer, (c) anti-leukemia cancer

Fig. 5(a) — Interaction of 3-fluorobenzamide against anti-ovarian cancer

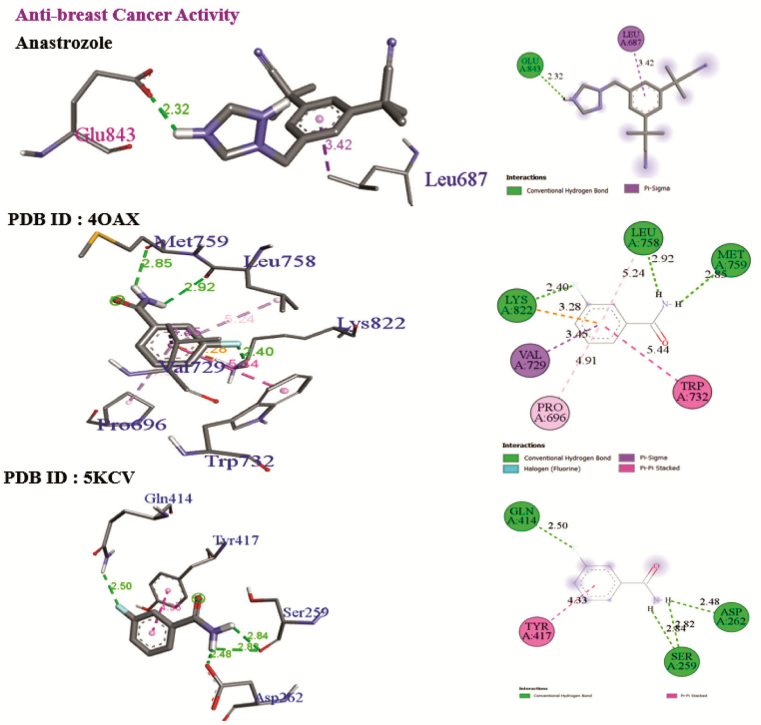

Fig. 5(b) — Interaction of 3-fluorobenzamide against anti-breast cancer

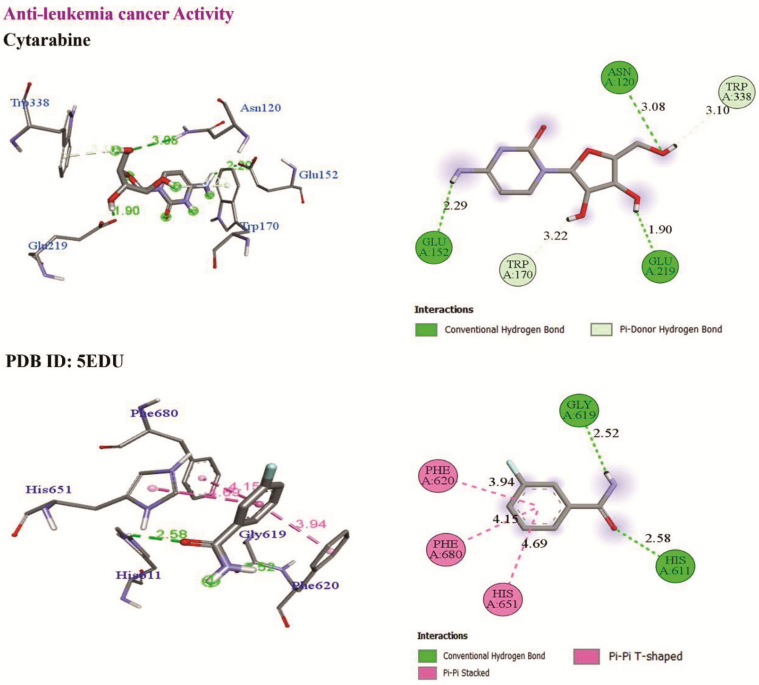

Fig. 5(c) — Interaction of 3-fluorobenzamide against anti-leukemia cancer

Table 5 — Docking calculation depicting interacting residues, binding site residues involved in H-bonding along with interacting residues

S. No.	Protein	Binding Energy (Kcal·mol)	Interacted Residues	Ligand and amino acids involved in H-bonding	Standard drugs	Binding Energy (Kcal·mol)	Interacted Residues	Drug and amino acids involved in H-bonding
1	7XJO	−6.5	HIS A:121, ALA A:140, ALA A:137, LEU A:138, THR A:144, TYR A:143	ALA A:140, ALA A:137, LEU A:138, THR A:144	Carboplatin (Anti-ovarian Cancer)	−5.1	LEU A: 138, ALA A: 137, THR A: 144, TYR A: 143, LEU A: 117	LEU A: 138, ALA A: 137, THR A: 144
2	7XGJ	−6.5	PRO A:141, ALA A:140, LEU A:138, TYR A:143, LEU A:83,THR A:144, VAL A: 118, IS A:121	ALA A:140, LEU A:138, THR A:144				
3	4OAR	−6.6	LYS A:822, LEU A:758, MET A:759, TRP A:732, PRO A:696, VAL A:729, LYS A: 822	LEU A: 758, MET A: 759, LYS A:822	Anastrozole (Anti-breast Cancer)	−5.9	LEU A; 687, GLU A: 843	GLU A: 843
4	5KCV	−5.4	GLN A:414, ASP A: 262, SER A:259, TYR A:417	GLN A: 414, ASP A:262, SER A:259				
5	5EDU	−6.5	PHE A:620, PHE A:680, HIS A:651, HIS A:611, GLY A:619	HIS A:611, GLY A:619	Cytarabine (Anti-leukemia Cancer)	−6.3	TRP A:338, ASN A:120, GLU A:219, TRP A: 170, GLU A: 152	ASN A:120, GLU A:219, GLU A: 152

Table 6 — ADMET profile of 3-fluorobenzamide and standard drugs

ADMET prediction	3FBA	Carboplatin	Anastrozole	Cytarabine	ADMET prediction	3FBA	Carboplatin	Anastrozole	Cytarabine
CaCo-2 permeability (log Papp in 10^{-6} cm/s)	1.215	−0.692	1.022	−0.082	P-glycoprotein substrate	No	No	No	No
Intestinal absorption (human) (%)	83.946	27.654	98.775	58.476	P-glycoprotein I inhibitor	No	No	No	No
Skin Permeability (log Kp)	−2.832	−2.735	−2.691	−2.742	P-glycoprotein II inhibitor	No	No	No	No
VDss (human) (log L/kg)	−0.153	−1.2	−0.097	0.136	Total Clearance (log mL/min/kg)	0.154	0.848	1.525	0.503
Fraction unbound (human) (Fu)	0.504	0.511	0.163	0.868	Renal OCT2 substrate	No	No	No	No
BBB permeability (log BB)	−0.256	−0.433	−0.347	−0.784	AMES toxicity test	No	No	Yes	No
CNS permeability (log PS)	−2.055	−3.105	−2.736	−3.665	Max. tolerated dose (human) (log mg/kg/day)	1.116	0.204	0.003	0.358
CYP2D6 substrate	No	No	No	No	hERG I inhibitor	No	No	No	No
CYP3A4 substrate	No	No	Yes	No	hERG II inhibitor	No	No	No	No
CYP1A2 inhibitior	No	No	Yes	No	Oral Rat Acute Toxicity (LD50) (mol/kg)	2.004	1.721	2.363	1.973
CYP2C19 inhibitior	No	No	Yes	No	Oral Rat Chronic Toxicity (LOAEL) (log mg/kg_bw/day)	2.562	2.247	1.338	2.98
CYP2C9 inhibitior	No	No	No	No	Hepatotoxicity	No	No	Yes	No
CYP2D6 inhibitior	No	No	No	No	Skin Sensitisation	No	No	No	No
CYP3A4 inhibitior	No	No	No	No	T.Pyriformistoxicity (log ug/L)	0.048	0.271	1.69	0.284
Carcinogenicity	No	No	No	No	Minnow toxicity (log mM)	2.272	1.408	1.205	4.221
Molecular weight (g/mol)	139.13	371.25	293.37	243.22	No. of Hydrogen bond acceptors	2	6	4	6
log P (octonal-water partition coefficient)	1.22	0.00	2.25	0.32	No. of Hydrogen bond donors	1	4	4	4

of all anti-ovarian, anti-breast and anti-leukemia cancer activities.

ADMET Prediction

Through the use of in silico ADMET analysis, it is possible to determine with sufficient efficacy whether a molecule has adequate pharmacokinetic features.[41] The bioavailability and toxicity concerns related to 3FBA have been predicted using the ADMET profile. The ADMET-SAR service indicates a higher human intestine absorption score (83.946%) for the substance. The LD50 is a crucial factor to take into account when evaluating the signs of poisoning that occur after an acute dosage in humans. The chemical has demonstrated exceptionally high blood-brain barrier (BBB) penetration of −0.256 for 3FBA, with a low LD50of 2.004 mol/kg. Moreover, several ADMET parameters of 3FBA in comparison to conventional drugs are shown in Table 6, indicating that the molecule satisfies with the standard results. Accordingly, the 3FBA findings demonstrated the good blood-brain barrier bridging, a high proportion

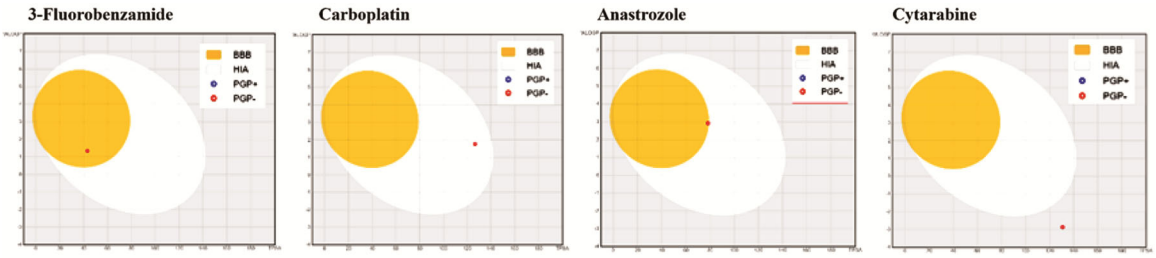

Fig. 6 — Boiled egg images of 3-fluorobenzamide and standard drugs

of plasma protein binding, and a reasonable chance of intestinal absorption by humans. As one of the five conditions stipulated by the Lipinski's rule of five[42], a chemical must not violate any, or at least one of the following five conditions, in order to be classified as a possible drug. The following criteria must be met: Molecular weight less than 500, number of acceptors less than 10, number of hydrogen bond donors less than 5, and log P (octonal-water partition coefficient) less than 5. Lipinski's rule of five has been applied to the molecule under investigation, as shown by Table 6. It was discovered that the molecule has a molecular weight of 139.13 (g/mole). The findings show that there is two hydrogen bond acceptors, one hydrogen bond donor and log P of 1.22 in the 3FBA by using SwissADME website. Further, the BBB penetration of 3FBA and its intestinal absorption is also confirmed via the BOILED-Egg model.[43] The physicochemical space that is most likely to produce brain penetration is represented by the yolk as shown in Fig. 6, whereas the white region indicates physicochemical space that is more likely to be passively absorbed through the gastrointestinal system. It revealed that the 3FBA molecule is found inside the yolk portion, demonstrating its intestinal absorption, BBB penetration and also consistent with typical medications, as seen in Fig. 6. Therefore, this suggested that the chemical may readily pass through the intestinal lining and reach the cell membrane.

Conclusions

The DFT/B3LYP approach with 6-31++G(d,p) and 6-311++G(d,p) basis sets are used to calculate the geometrical parameters and to analyze the normal mode of 3-fluorobenzamide. There is good agreement between the computed and observed parameters. By analyzing the lower energy gap in the gas phase, methanol and ethanol (5.52, 5.57, and 5.57 eV) indicates the chemical reactivity of the molecule. The global reactivity descriptors and DOS spectra have been analyzed. The maximum likely targets for both electrophilic and nucleophilic assaults have been determined to be the oxygen, nitrogen, and hydrogen atoms. These atoms are also shown on the MEP plot and may be verified by the use of the Fukui functions and Mulliken charges studies. The NMR shift values for the carbon and proton in the molecule have been calculated. 3FBA has been shown to have the strongest interaction with the ovarian, breast and leukemia cancer proteins, 7XJO, 7XGJ, 4OAR, 5KCV and 5EDU exhibiting the highest affinity energy value of −6.5, −6.5, −6.6, −5.4 and −6.5 Kcal·mol^{-1}, respectively. These are comparable with the binding affinity of standard drugs, carboplatin, anastrozole and cytarabine. Furthermore, ADMET research indicates that 3FBA will successfully treat ovarian, breast and leukemia malignancies and decrease the side effects of medical operations.

Supplementary Data

Supplementary data of this article is available at https://nopr.niscpr.res.in/handle/123456789/63168

Conflict of interest

There are no conflicts to declare.

References

1 Aki-Sener E, Bingoel K K, Temiz-Arpaci O, Yalcin I & Altanlar N, Synthesis and microbiological activity of some N-(2-Hydroxy-4-substitutedphenyl) benzamides, phenylacetamides and furamides as the possible metabolites of antimicrobial active benzoxazoles, *Farmaco,* **57** (2002) 451–456.

2 Boonen J, Bronselaer A, Nielandt J, Veryser L, De Tré G & De Spiegeleer B, Alkamid database: Chemistry, occurrence and functionality of plant N-alkylamides, *J Ethnopharmacol*, **142** (2012) 563–590.

3 Wanjari P M, Mokale S N, Bharati A V & Ingle V N, Theoretical and experimental verification of molecular properties of novel benzamide derivatives using computational platforms and *in vitro* antibacterial activity, *Med Chem Res*, **30** (2021) 655–663.

4 Stark D, Piel M, Hübner H, Gmeiner P, Gründer G & Frank R, *In vitro* affinities of various halogenated benzamide derivatives as potential radioligands for non-invasive

quantification of 2-like dopamine receptors, *Bioorg Med Chem*, **15** (2007) 6819–6829.

5 Al-Otaibi J S, Mary Y S, Mary Y S, Thirunavukkarasu M, Trivedi R & Chakraborty B, Conformational, reactivity analysis, wave function-based properties, molecular docking and simulations of a benzamide derivative with potential antitumor activity-DFT and MD simulations, *Polycycl Aromat Compd*, **43** (2022) 2015–2031.

6 Prabukanthan P, Bhakyajothi V, Kumar M S & Dinakaran K, Physicochemical and DFT studies of organic NLO single crystal 4-methoxy-N-(2-methyl-5-nitrophenyl) benzamide, *Mol Cryst Liq Cryst*, **754** (2022) 43–67.

7 Rizk M G, Emara A A A & Mahmoud N H, Spectroscopic studies, DFT calculations, thermal analysis, anti-cancer evaluation of new metal complexes of 2-hydroxy-N-(4-phenylthiazol-2-yl) benzamide, *J Mol Struct*, **1246** (2021) 131143.

8 Raja G, Venkatesh G, Al-Otaibi J S, Vennila P, Mary Y S & Lopez Y S, Synthesis, characterization, molecular docking and molecular dynamics simulations of benzamide derivatives as potential anti-ovarian cancer agents, *J Mol Struct*, **1269** (2022) 133785.

9 Mohammed A M & Emam H F, Synthesis, crystal structure, DFT calculation and Hirshfeld surface analysis of N-(4-methyl phenyl)-2-(3-nitro-benzamido) benzamide, *Bull Chem Soc Ethiop*, **38** (2023) 229–239.

10 Frisch M J, Trucks G W, Schlegel H B, Scuseria G E, Robb M A, Cheeseman J R, Scalmani G, Barone V, Petersson G A, Nakatsuji H, Li X, Caricato M, Marenich A, Bloino J, Janesko B G, Gomperts R, Mennucci B, Hratchian H P, Ortiz J V, Izmaylov A F, Sonnenberg J L, Williams-Young D, Ding F, Lipparini F, Egidi F, Goings J, Peng B, Petrone A, Henderson T, Ranasinghe D, Zakrzewski V G, Gao J, Rega N, Zheng G, Liang W, Hada M, Ehara M, Toyota K, Fukuda R, Hasegawa J, Ishida M, Nakajima T, Honda Y, Kitao O, Nakai H, Vreven T, Throssell K, Jr. Montgomery J A, Peralta J E, Ogliaro F, Bearpark M, Heyd J J, Brothers E, Kudin K N, Staroverov V N, Keith T, Kobayashi R, Normand J, Raghavachari K, Rendell A, Burant J C, Iyengar S S, Tomasi J, Cossi M, Millam J M, Klene M, Adamo C, Cammi R, Ochterski J W, Martin R L, Morokuma K, Farkas O, Foresman J B & Fox D J, C T Gaussian 09.2013 Gaussian 09, Revision A.02 (Gaussian, Inc., Wallingford), 2016.

11 Frisch A, Neilson A B & Holder A J, GAUSSVIEW User Manual (Pittsburgh, CT: Gaussian Inc) 2009.

12 Jamroz M H, Vibrational energy distribution analysis: VEDA 4 Program (Warsaw, Poland) 2004.

13 Subhashandrabose S, Akhil R, Krishnan R, Saleem H, Parameswari R, Sundaraganesan N, Thanikachalam V & Manikandan G, Vibrational spectroscopic Study and NBO analysis on bis(4-amino-5-mercapto-1,bib2,4-triazol-3-yl) methane using DFT method, *Spectrochim Acta A Mol Biomol Spectrosc*, **77** (2010) 877–884.

14 Barfiled M & Fagerness P, Density functional theory/GIAO studies of the ^{13}C, 15N, and ^{1}H NMR chemical shifts in aminopyrimidines and aminobenzenes: relationships to electron densities and amine group orientations, *J Am Chem Soc*, **119** (1977) 8699–8711.

15 O'boyle N M, Tenderholt A L & Langner K M, Cclib: A library for package-independent computational chemistry algorithms, *J Comput Chem*, **29** (2007) 839–845.

16 Seeliger D & de Groot B L, Ligand docking and binding site analysis with PyMOL and Autodock/Vina, *J Comput Aided Mol Des*, **24** (2010) 417–422.

17 Trott O & Olson A J, AutoDockVina: improving the speed and accuracy of docking with a new scoring function, efficient optimization, and multithreading, *J Comput Chem*, **31** (2009) 455–461.

18 BIOVIA D S, Discovery Studio Modeling Environment; Release 2017, Dessault Systemes (San Diego, CA, USA) 2017.

19 Kim S, Thiessen P A, Bolton E E, Chen J, Fu G, Gindulyte A, Han L, He J, He S, Shoemaker B A, Wang J, Yu B, Zhang J & Bryant S H, Pubchem substance and compound databases, *Nucleic Acids Res*, **44** (2016) D1202–D1213.

20 Jia C Y, Li J Y, Hao G F & Yang G F, A drug-likeness toolbox facilitates ADMET study in drug discovery, *Drug Discov*, **25** (2020) 248–258.

21 Daina A, Michielin O & Zoete V, SwissADME: A Free Web Tool to Evaluate Pharmacokinetics, Drug-Likeness and Medicinal Chemistry Friendliness of Small Molecules, *Sci Rep*, **7** (2017) 42717.

22 Saeed A, Khera R A, Abbas N & Florke U, N-Cyclohexyl-3-fluorobenzamide, *Acta Cryst*, **E64** (2008) o2209.

23 Merrick J P, Moran D & Radom L, An evaluation of harmonic vibrational frequency scale factors, *J Phys Chem A*, **111** (2007) 11683–11700.

24 Karabacak M, Kurt M, Cinar M, Ayyappan S, Sudha S & Sundaraganesan N, The spectroscopic (FT-IR, FT-Raman, UV) and first order hyperpolarizability, HOMO and LUMO analysis of 3-aminobenzophenone by density functional method, *Spectrochim Acta A Mol Biomol Spectrosc*, **15** (2012) 365–376.

25 Govindarajan M, Karabacak M, Suvitha A & Periandy S, FT-IR, FTRaman, ab initio, HF and DFT studies NBO, HOMO-LUMO and electronic structure calculations on 4-chloro-3-nitrotoluence, *Spectrochim Acta A Mol Biomol Spectrosc*, **89** (2012) 137–148.

26 Kunjumol V S, Jeyavijayan S, Sumathi S & Karthik N, Spectroscopic, computational, cytotoxicity, and docking studies of 6-bromobenzimidazole as anti-breast cancer agent, *J Mol Recognit*, **37** (2024) e3074.

27 YossaKamsi R A, Ejuh G W, Tadjouteu A Y, Njeumen C A, Tchoffo F & Ndjaka J M B, Computational study of reactivity and solubility of Rubescin D and E molecules in gas phase and in solvent media using Hartree-Fock and DFT methods, *Chin J Phys*, 60 (2019) 1–11.

28 Jeyavijayan S, Molecular structure, spectroscopic (FTIR, FT-Raman, 13C and 1H NMR, UV), polarizability and first-order hyperpolarizability, HOMO–LUMO analysis of 2,4-difluoroacetophenone, *Spectrochim Acta A Mol Biomol Spectrosc*, **136** (2015) 553–566.

29 Szafran M, Komasa A & Bartoszak-Adamska E, Crystal and molecular structure of 4-carboxypiperidinium chloride (4-piperidinecarboxylic acid hydrochloride), *J Mol Struct*, **827** (2007) 101–107.

30 Ayers P W & Parr R G, Variational principles for describing chemical reactions: the Fukui function and chemical hardness revisited, *J Am Chem Soc*, **122** (2000) 2010–2018.

31 Morell C, Grand A & Toro-Labbé A, New dual descriptor for chemical reactivity, *J Phys Chem A*, **109** (2004) 205–212.

32 Karrouchi K, Brandán S A, Sert Y, El-marzouqi H, Radi S, Ferbinteanu M, Faouzi M E A, Garcia Y & Ansar M, Synthesis, X-ray structure, vibrational spectroscopy, DFT, biological evaluation and molecular docking studies of (E)-N'-(4-(dimethylamino)benzylidene)-5-methyl-1h-pyrazole-3-carbohydrazide, *J Mol Struct*, **1219** (2020) 128541.

33 Ourhzif E M, MostafaKetatni E, Akssira M, Troin Y & Khouili M, Crystal structure, Hirshfeld surface analysis and DFT studies of Euphorbioside monohydrate a major bisnorsesquiterpene isolated from Euphorbia resinifera latex, *J Mol Struct*, **1241** (2021) 130511.

34 Fizer M, Slivka M, Korol N & Fizer O, Identifying and explaining the regioselectivity of Alkylation of 1,2,4-Triazole-3-Thiones Using NMR, GIAO and DFT Methods, *J Mol Struct*, **1223** (2021) 128973.

35 Tiwari G, Sharma D & Singh N B, Electronic structure and molecular docking studies of an anti-HIV drug stavudine, *J Sci Ind Res*, **79** (2020) 337–339.

36 Pattanaik S, Nandi S, Swain R, Sahoo R N, Nanda A & Mallick S, Effect of quaternary ammonium surfactant on buccal permeation of budesonide film formulation: In silico docking studies, *J Sci Ind Res*, **81** (2022) 1259–1266.

37 Alghuwainem Y A A, Abd El-Lateef H M, Khalaf M M, Abdelhamid A A, Alfarsi A, Gouda M, Abdelbaset M & Abdou A, Synthesis, structural, DFT, antibacterial, antifungal, anti-inflammatory, and molecular docking analysis of new VO(II), Fe(III), Mn(II), Zn(II), and Ag(I) complexes based on 4-((2-hydroxy-1-naphthyl)azo) benzenesulfonamide, *J Mol Liq*, **369** (2023) 120936.

38 Dawooda M, Elbadawia M, Böckersa M, Bringmann G & Efferth T, Molecular docking-based virtual drug screening revealing an oxofluorenylbenzamide and a bromonaphthalene sulfonamide hydroxybenzoic acid as HDAC6 inhibitors with cytotoxicity against leukemia cells, *Biomed Pharmacother*, **129** (2020) 110454.

39 Usha Rani K, Sharma G V M, Saxena S, Guruprasad L & Padmavathi D A, Synthesis, DFT and molecular docking study of novel bis 1,2,3-triazole derivatives of 2-hydroxyquinoline-4-carboxylate as antimicrobial agents, *Indian J Biochem Biophys*, **60** (2023) 729–740.

40 Meenakumari V, Mangaiyarkkarasi J, Premkumar R, Mohamed A R, Milton F B A & Thenmozhi N, Spectroscopic characterization, quantum chemical and molecular docking investigations on methyl indole-3-carboxylate: A potent cervical cancer drug, *J Mol Struct*, **1305** (2024) 137711.

41 Trilaksana H, Thanmayalaxmi D & Suvitha A, ADMET, pharmacokinetic and docking properties of the fungal drug 2-(2,4-difluorophenyl)-1,3-bis(1,2,4-triazol-1-yl)propan-2-ol by using quantum computational methods, *Indian J Biochem Biophys*, **60** (2023) 58–64.

42 Lipinski C A, Lead- and drug-like compounds: the rule-of-five revolution, *Drug Discov Today Technol*, **1** (2004) 337–341.

43 Daina A, Zoete V, A BOILED-Egg to predict gastrointestinal absorption and brain penetration of small molecules, *Chem Med Chem*, **11** (2016) 1117–1121.